

High-precision heat-capacity study of phase transitions in a lyotropic liquid crystal

S. T. Shin, Satyendra Kumar, and D. Finotello

Department of Physics and Liquid Crystal Institute, Kent State University, Kent, Ohio 44242

S. Sabol Keast and M. E. Neubert

Liquid Crystal Institute, Kent State University, Kent, Ohio 44242

(Received 16 December 1991)

The nematic to neat-soap (N -NS) and nematic to isotropic (N - I) phase transitions in binary solutions of cesium per-fluoro-octanoate (CsPFO) and water have been studied by high-precision calorimetry at 39.3, 43.6, 48.3, 49.0, 50.7, 52.0, and 55.3 wt. % CsPFO concentrations. The ratio of the heat-capacity amplitudes, above and below the N -NS transition, and the critical exponent α remain near 1 and 0, respectively, suggesting three-dimensional XY -type behavior. The coexistence range and the latent heat at the first-order N - I transition decrease with decreasing concentration. Extrapolation of the N - I coexistence width suggests existence of a Landau point at ~ 28 wt. % concentration. The coefficients of expansion in the Landau-de Gennes free energy at the N - I transition and their concentration dependence have been determined. Coefficients of the cubic and the biquadratic terms become vanishingly small at low concentrations underscoring the need to use higher-order terms in the free energy.

PACS number(s): 64.70.Md, 64.60.Fr, 82.60.Fa

INTRODUCTION

The cesium per-fluoro-octanoate (CsPFO) molecules, like a typical surfactant, have hydrophobic and hydrophilic ends. They aggregate to form dislike micelles [1] of positive diamagnetic anisotropy when dissolved in water at concentrations higher than the critical micellar concentration. At high concentrations (> 20 wt. % CsPFO), the disk-shaped micelles develop orientational and one-dimensional translational order to form the nematic (N) and the neat-soap (NS) phases [1], respectively. At a fixed concentration, such systems undergo phase transitions with decreasing temperature from the completely disordered isotropic (I) phase to the N phase, and from the N phase to the NS phase.

On the basis of their structure and symmetry, the N and NS phases exhibited by lyotropic systems can be considered similar to the thermotropic N and smectic- A phases. The N - I and N -NS phase transitions of such systems have frequently been compared with the corresponding thermotropic liquid-crystal transitions. Many experimental studies have been undertaken to comprehend the microscopic structure of these phases and the nature of the N -NS and N - I transitions. Previous optical [2], quasielastic light-scattering [2,3], magnetic-birefringence [4,5], magnetic-deformation [6], conventional [7] and synchrotron [5] x-ray diffraction, small-angle neutron-scattering [8], and electrical-conductivity [9] studies have provided evidence in favor of the lyotropic liquid crystals being analogous to the thermotropic materials. There is now substantial quantitative evidence which can be used to argue against the conventional bilayer structure of the neat-soap phase (at least in some cases), and in favor of arrangement of the micelles to form a layered structure. The lyotropic systems differ

from the thermotropics in one regard. The microscopic entity that undergoes ordering in lyotropic liquid crystals is an aggregate (micelle) of 50–100 molecules while in thermotropic materials it is the individual molecules that form liquid-crystalline phases. The neat-soap (or smectic- A) fluctuations in the nematic phase diverge [2] anisotropically with critical exponents $\nu_{\parallel}=0.72\pm 0.1$, and $\nu_{\perp}=0.58\pm 0.1$, for the CsPFO plus water system. At the N - I transition, $\beta=0.5\pm 0.1$ and $\gamma=1$ is obtained [2,5], in agreement with mean-field theory. These results are similar to those obtained for many thermotropic liquid crystals.

The phase diagram for the CsPFO plus water system has been determined with high precision by Boden *et al.* [1]. In their NMR experiments, they found that the N -NS transition changed from second order at low concentrations to first order at high concentrations. The tricritical point, at which the N -NS transition changes from second order to first order, was determined to be near 57 wt. %. In a later study [10], with better temperature precision, this concentration was revised to a significantly lower value, ~ 43 wt. %. Their experiments also supported the possibility of a Landau point at the N - I transition at low concentrations in accordance with earlier reports based on light-scattering [2] and magnetic-birefringence experiments [4,5]. Unfortunately, most of the measurements made to this date (for example, light and x-ray diffraction, optical, magnetic deformation, etc.) depend on the ability to align and/or to reorient the micelles, which is inherently difficult due to slow relaxation processes in these materials. Furthermore, almost all of their physical properties (dielectric and diamagnetic anisotropy, optical birefringence, etc.) are more than two orders of magnitude smaller than in thermotropic liquid crystals, making it even harder to conduct high-precision

measurements.

We decided to use the heat-capacity (C_p) technique to conduct a comprehensive study of phase transitions in the CsPFO plus water system. The heat-capacity measurements are independent of the macroscopic alignment and reorientational times of the micelles and offer an opportunity to obtain more reliable results than possible with other techniques. Previous heat-capacity studies [11,12] have provided very useful qualitative information about the behavior of the heat capacity of this system. The changes in heat capacity in these materials were nearly 300–500 times smaller than those found in thermotropic liquid crystals, e.g., 4-(*n*-octyloxy)-4'-cyanobiphenyl (8OCB) [13]. In these experiments, the solutions remained homogeneous for a long time and did not require stirring during the scans. Heating and cooling scans were found to be essentially the same.

We performed heat-capacity measurements on seven different concentrations. Our results, a summary of which was published elsewhere [14], show that the *N*-*NS* transition is in agreement with predictions of the three-dimensional *XY* (3D-*XY*) model. We could not observe the evolution of the heat-capacity exponent α toward the tricritical value of $\frac{1}{2}$ because of transition broadening due to impurities. The coexistence previously observed [1,10] may have been due to the same reason, rather than the presence of a tricritical point. We have also determined the latent heat, the width of the coexistence region, and the fluctuation heat capacity at the *N*-*I* transition. The concentration dependence of these quantities shows that the transition line should terminate at a Landau point at ~ 28 wt. % concentration. A calculation of the coefficients in the Landau-de Gennes free energy emphasizes the need to include higher than biquadratic terms for a better description of this transition.

EXPERIMENTAL DETAILS

Cesium per-fluoro-octanoate was synthesized by stirring and heating equimolar amounts of pentadecafluoro-octanoic acid and cesium hydroxide (both from Aldrich Chemical Co.) until all the material turned to foam. The wet solid was dried in a vacuum oven, dissolved in isopropyl alcohol, cooled, and filtered. Recrystallization was repeated in this manner two more times to produce the purified CsPFO. The samples were prepared by dissolving CsPFO in distilled and deionized water. The transition temperatures for the concentrations studied, and shown in Fig. 1, are in good agreement with published [1,10] values.

Heat-capacity measurements of lyotropic materials are particularly difficult because of the small changes involved and a number of other technical reasons. For instance, it is crucial to seal the samples so that no solvent evaporation and, hence, drift of transition temperatures occurs. The cell has to be made from chemically inert and corrosion-resistant materials with suitable thermal properties.

We used a scanning microcalorimeter, model MC-2, manufactured by Microcal, Inc., to measure the changes

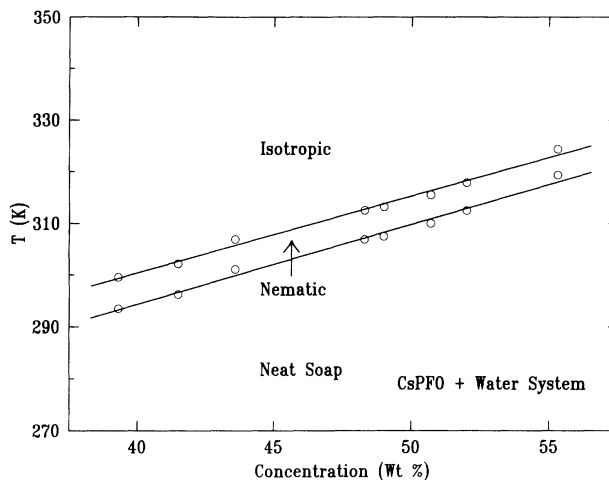


FIG. 1. Partial phase diagram of the cesium per-fluoro-octanoate plus water system. The open circles indicate the transition temperatures obtained for the concentrations used in this study. The solid lines are drawn as a guide to the eye.

in the heat capacity as a function of temperature. The sample and reference cells of this calorimeter (Fig. 2) are made of tantalum metal with a 1.2-ml volume (1.6 to 1.8 g of CsPFO solutions). This calorimeter's sample and reference cells are connected to sealed reservoirs by 10-cm-long, 1.6-mm inner-diameter tubes. This prevents sample evaporation and provides an escape path for air bubbles formed during the filling process. The sample and reference cells are enclosed in an adiabatic chamber made of an evacuated jacket. A syringe with a long hypodermic needle was used to fill the cells. Enough material was injected into these cells so that between a quarter to a half of the reservoirs were also filled. The reservoirs were tightly sealed with O-rings and a stainless-steel disk. Power was supplied to the main heaters attached to the two cells to raise their temperature at a predetermined rate. The temperature of the adiabatic chamber was also raised at the same rate with the help of main and feedback heaters. The power to the feedback heater attached to the jacket is determined by a 20-junction thermopile which senses the temperature difference between the cells and the jacket. A 100-junction thermopile was used to detect the temperature difference between the sample and the reference cells, and to provide a differential power signal to the cell feedback heaters and maintain them at the same temperature. The differential power was a direct measure of C_p , and was recorded as a function of temperature.

This calorimeter allows accurate measurements of small changes in C_p because of the large sample mass and background C_p compensation with a reference material (water in our case). It has a maximum sensitivity of 15 $\mu\text{cal}/\text{min}$ and an operating temperature range from -30°C to 120°C . The temperature resolution of the calorimeter is better than 7 mK at the scan rates used in our study. The scan rate can be set between 11 mK/min and 1.5 K/min. Signal averaging over several seconds

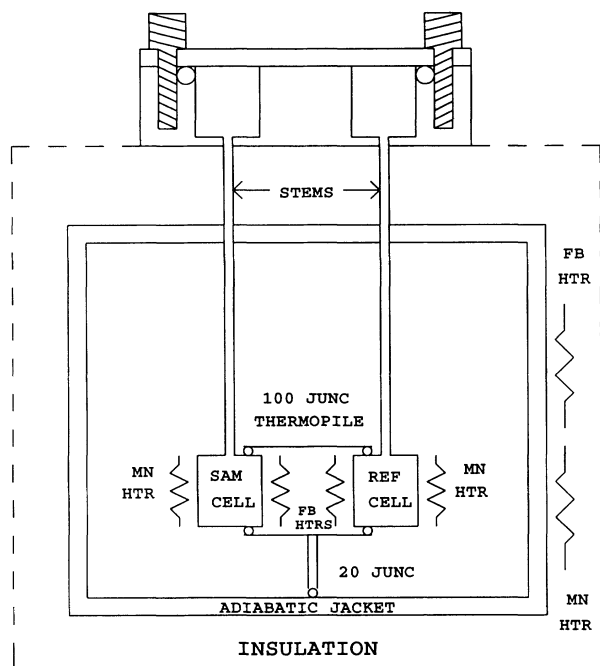


FIG. 2. Schematic diagram of the adiabatic chamber and sample and reference cells of the scanning calorimeter. The main (MN) and feedback (FB) heaters (HTR) are used to change temperatures of the adiabatic chamber and the sample (SAM) and reference (REF) cells at the same rate. The 100- and 20-junction (JUNC) thermopiles are used to sense temperature differences and to control the amount of heating power supplied to the feedback heaters.

was performed to improve the signal-to-noise ratio. The experimental error in C_p was taken to be $\frac{1}{4}$ of the scatter in the data points in a straight section of the heat-capacity curve.

At the time these measurements were made, we did not have the capability to perform cooling scans to check for any hysteresis, monotropic phases, or other time-dependent effects, such as coalescence of micelles at low temperatures. Very recently, the calorimeter has been modified to perform cooling scans. We have now verified that the heating and cooling scans on these mixtures yield the same results, although the cooling scans tend to have higher noise due to technical reasons. After an initial period of a few days, the scans are reproducible to a high degree. In one instance, two scans taken four months apart were found to be identical within experimental resolution, and without a measurable change in the transition temperatures, emphasizing the chemical and thermodynamic stability of these systems.

Thermal equilibration was a concern given the large samples used in this calorimeter. We found in our initial studies that the results were independent of the scan rate at rates slower than 50 mK/min. Hence, all of our scans, except for 39.3 wt. % sample, were taken at heating rates between 11 and 20 mK/min. A scan rate of 37 mK/min was used for the most dilute (39.3%) mixture. The N - NS transition for this sample is near room temperature

which makes it difficult to control the scan rate and to scan at a slower rate. This appears to be responsible for minor deviations of the results for 39.3% solution from the general trends determined by other mixtures. Experimentally measured [15] densities of these mixtures were used in converting the data to units of J/g K.

DATA ANALYSIS

In the analysis of the N - NS transition, the use of correction-to-scaling [16] term was found necessary as the fits without it required drastically different values of the heat-capacity amplitude and the critical exponent above and below the N - NS transition. The function

$$C_p(t) = (A^\pm/\alpha)t^{-\alpha}(1 + D^\pm t^{0.5}) + C(t')^{-\alpha'} + ET + B \quad (1)$$

described very well the measured heat capacity below the N - I transition as evident from the fit to a scan for the 43.6 wt. % mixture (Fig. 3). The values of the coefficients A and D were allowed to be different above (+) and below (-) the transition. In Eq. (1), the first term represents a power-law divergence with first correction-to-scaling term. The reduced temperature is $t = |T - T_{N-NS}|/T_{N-NS}$, and $t' = |T - T_c^{**}|/T_c^{**}$, T_c^{**} is the virtual second-order N - I transition (superheating) temperature; α is the heat-capacity exponent while α' represents the power-law increase in heat capacity at the N - I transition. As discussed later, α' should be considered only as a fit parameter and not as the critical exponent for the N - I transition. This term accounts for part of the background heat capacity for the N - NS transition. The last two terms, with T in kelvins, provide a linear background. The constant B represents the sum of the regular and the critical background heat capacities.

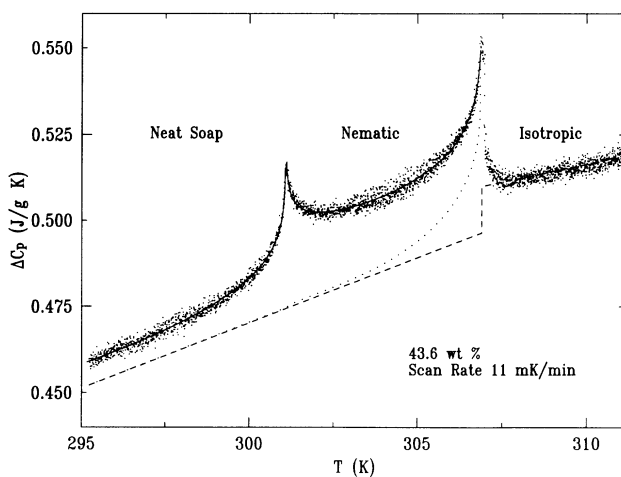


FIG. 3. ΔC_p vs temperature for the 43.6 wt. % CsPFO plus water mixture. The solid line is a fit to Eq. (1) and the dotted line represents C_p with $t^{-\alpha}=1$ in the first term, as described in the text. The dashed line is the background for the N - I transition obtained with the first analysis method (see text).

The background heat capacity at the N - NS transition, due to the diverging heat capacity at T_{N-I} , was also approximated by a second-order polynomial, instead of the power law ($t'^{-\alpha}$) that appears in Eq. (1). Alternatively, a linear background in the NS region was determined graphically by drawing a tangent to the C_p curve, well below the N - NS transition. This background was subtracted from the data. Then, only the first (divergent) term with correction-to-scaling and a constant background term were used to fit data below the minimum in the N region. These fitting methods and several variations of them were attempted. The values of the critical exponent α and the ratio of specific-heat amplitudes A^+/A^- varied negligibly for fits over the same temperature range from those obtained with the first, more intuitive method, described in the preceding paragraph. However, χ^2 was slightly higher and the fits were less stable with respect to temperature-range shrinking. The renormalization [17] form of the heat capacity, obtained by replacing the first term of Eq. (1) by $[A^\pm t^{-\alpha_R}/(1+B^\pm t^{-\alpha_R})]$, also did not give a stable α_R with temperature-range shrinking, suggesting that renormalization was not occurring.

The fits obtained with the C_p functional of Eq. (1) for all data below T_{N-I} , over a range larger than ± 5 K in most cases, are shown by solid lines in Figs. 3–5. The values of the parameters C , t' , α' , E , and B that determine the background heat capacity for the N - NS transition were fixed at the best-fit values. The data were then

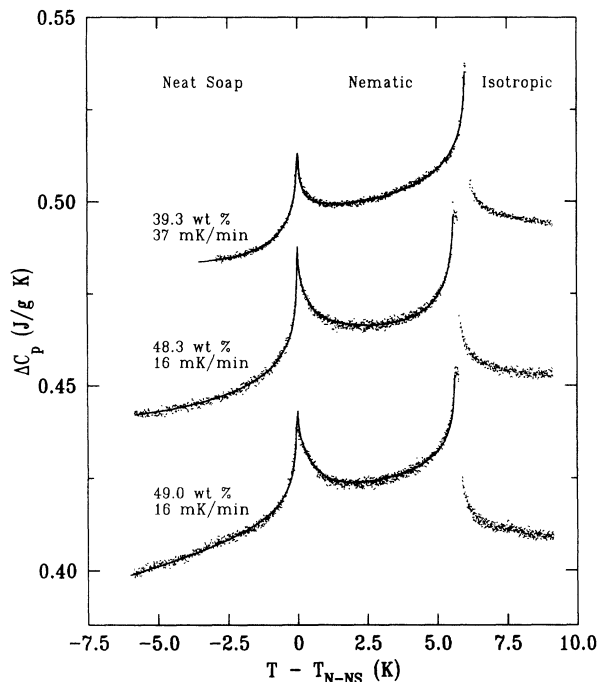


FIG. 4. ΔC_p vs $T - T_{N-NS}$ for 39.3, 48.3, and 49.0 wt. % mixtures. The solid lines are fits to the data below T_{N-I} , as described in the text. The data for 48.3 and 49.0 wt. % have been shifted down, for clarity, by 0.08 and 0.11 J/g K, respectively. Note that the zero of the heat-capacity signal depends on instrument settings and is different for different scans. The heating scan rates for these concentrations are also indicated.

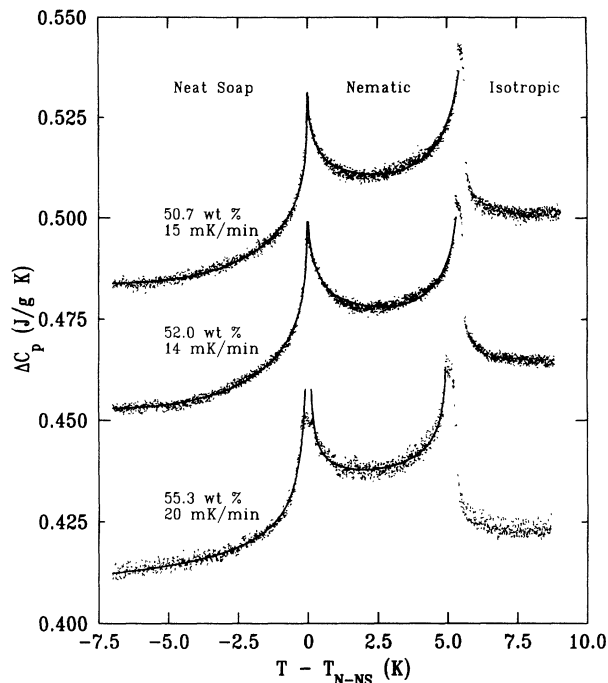


FIG. 5. Heat-capacity changes plotted against $T - T_{N-NS}$ for 50.7, 52.0, and 55.3 wt. % CsPFO solutions. The fits represented by the solid lines are discussed in the text. The data for 52.0 and 55.3 wt. % have been shifted down by 0.035 and 0.070 J/g K, respectively. The scan rates are also indicated.

refitted to Eq. (1) over a much narrower (± 1 K) range and only the parameters in the first term varied. The values of various parameters obtained from these fits are listed in Table I. Probable errors in the value of α were calculated by fixing α at values different from the best-fit value, and refitting the data to determine χ^2 . A parabola, with a minimum at the best-fit value of α , is obtained when χ^2 is plotted against the corresponding value of α as shown in Fig. 6 for the 43.6 wt. % mixture. The F test was used to determine 95% confidence limits on α . The possible uncertainties in the value of α , obtained in this manner and listed in Table I, were as high as 80%. Fits over several temperature ranges were attempted to determine the effect of range shrinking. The ratio A^+/A^- remained essentially unity irrespective of the temperature range. The value of α varied significantly, well beyond the probable errors given in Table I, with the temperature range selected. However, it never exceeded 0.006 except for the 55.3 wt. % solution, for which it remained nearly unchanged.

The N - NS transitions are sharp and well described by the function used in the fits for the 39.3, 43.6, and 48.3 wt. % solutions. Figures 7 and 8 show the data and fits, for all concentrations, over a ± 1 K range near the N - NS transition. The N and NS phases coexist at higher concentrations. The coexistence range (Fig. 8) increases from approximately 6 mK for 49.0 wt. % to 351 mK for 55.3 wt. %. The data in the coexistence region, shown by solid points, were excluded from the fits. A reliable estimation of α becomes difficult for these samples due to

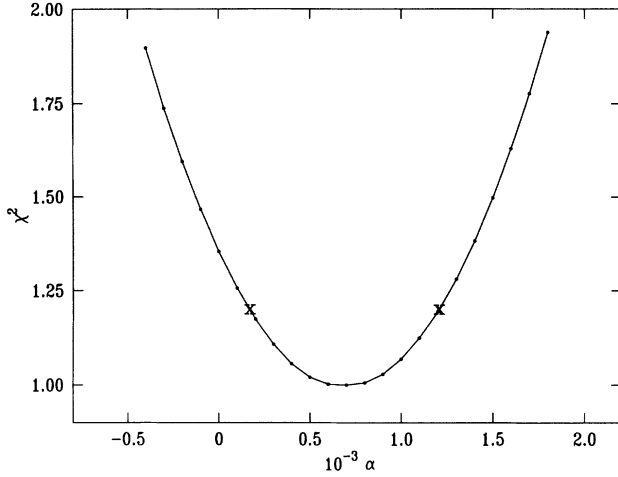


FIG. 6. χ^2 , a measure of goodness of fit, vs α for 43.6 wt. % solution. The X's mark the 95% confidence limits determined by the F test; $F(340,340) \cong 1.20$. The values of χ^2 have been normalized using its best-fit value.

the coexistence.

Analysis of the N - I transition was rendered particularly difficult by the close proximity of the N - NS transition, a wide N - I coexistence, and scant data representing pre-transitional effects above T_{N-I} . All of these factors conspired to make it practically impossible to obtain the true heat-capacity exponent for the N - I transition. It is, thus, more appropriate to consider α' , in the above analysis, as

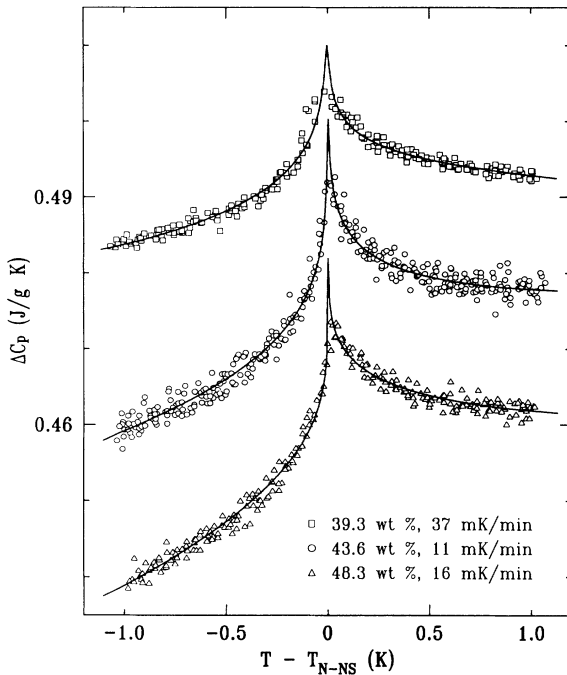


FIG. 7. ΔC_p vs $T - T_{N-NS}$ for 39.3, 43.6, and 48.3 wt. % samples, shown within ± 1 K of the N - NS transition. The solid lines are the best fits discussed in text. The plots for 43.6 and 48.3 wt. % have been shifted down for clarity by 0.025 and 0.050 J/g K, respectively.

TABLE I. Least-squares values of fitting parameters over the ± 1 K range for the nematic to neat-soap transition in cesium per-fluoro-octanoate plus water mixtures. Temperature-range shrinking gives a larger variation of α than the probable errors reported here and places an upper limit of 0.006 on α for all except the 55.3 wt. % solution for which it remains unchanged.

Conc. (wt. %)	T_{N-NS} (K)	T_c^{**} (K)	Reduced temp. range	A^+ (J/g K)	A^+/A^-	α	D^+	D^-/D^+	C (J/g K)	α'	E (J/g K ²)	B (J/g K)	χ^2
39.3	293.482	299.488	$6.5 \times 10^{-5} - 3 \times 10^{-3}$	0.0038 ± 0.0003	1.001	0.0006 ± 0.0002	0.0006	-17.4	1.22	0.005	-0.007	-7.02	0.98
43.6	301.080	306.903	$5.0 \times 10^{-5} - 3 \times 10^{-3}$	0.0041 ± 0.0003	1.001	0.0007 ± 0.0003	-0.004	6.71	1.85	0.005	0.0015	-7.47	1.09
48.3	306.862	312.509	$5.0 \times 10^{-5} - 3 \times 10^{-3}$	0.0022 ± 0.0003	1.003	0.0009 ± 0.0006	-0.025	1.74	2.36	0.003	0.0029	-5.20	1.49
49.0	307.438	313.121	$4.5 \times 10^{-5} - 3 \times 10^{-3}$	0.0020 ± 0.0001	1.003	0.0009 ± 0.0007	-0.101	1.01	2.85	0.002	0.0059	-6.34	2.60
50.7	309.946	315.444	$8.0 \times 10^{-5} - 3 \times 10^{-3}$	0.0042 ± 0.006	1.001	0.0012 ± 0.0009	-0.010	7.65	1.77	0.006	-0.0001	-4.67	1.30
52.0	312.418	317.820	$1.0 \times 10^{-4} - 3 \times 10^{-3}$	0.0051 ± 0.005	1.003	0.0031 ± 0.001	-0.011	12.34	1.26	0.007	0.0003	-2.50	1.28
55.3	319.306	324.352	$5.5 \times 10^{-4} - 3 \times 10^{-3}$	0.012 ± 0.0015	1.012	0.012 ± 0.004	0.011	1.25	1.82	0.002	0.0055	-4.19	0.91

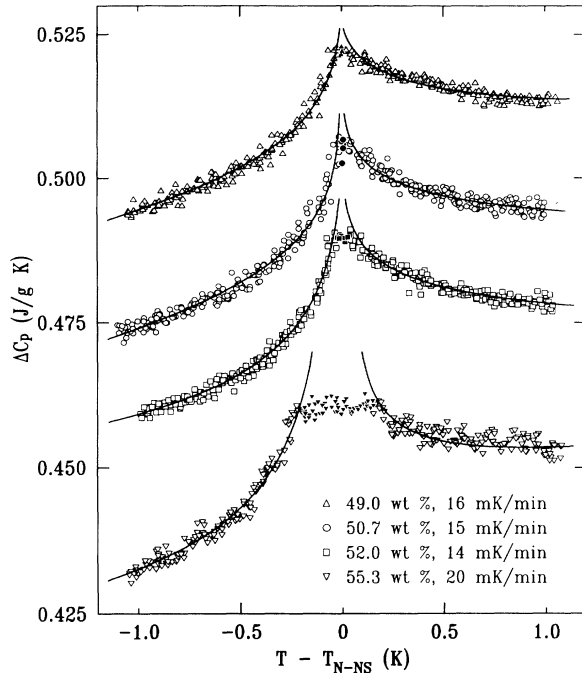


FIG. 8. ΔC_p vs $T - T_{N-NS}$ for 49.0, 50.7, 52.0, and 55.3 wt. % samples within ± 1 K of the $N-NS$ transition, taken at the indicated scan rates. The solid lines are the best fits discussed in the text. The filled symbols represent points in the coexistence regions of 6-, 21-, 77-, and 351-mK width for the 49.0, 50.7, 52.0, and 55.3 wt. % mixtures, respectively. The plots for 50.7, 52.0, and 55.3 wt. % have been shifted down for clarity by 0.02, 0.04, and 0.06 J/g K, respectively.

a fit parameter. However, it was possible to calculate the latent heat, total fluctuation heat capacity, and the $N-I$ coexistence range. We employed two methods to determine these quantities as described below.

In the *first method*, the power of t , in Eq. (1), was set to zero in order to remove the divergence associated with the $N-NS$ transition from the total heat capacity. The first term (with $t^{-\alpha}=1$) in Eq. (1), thus represented the heat capacity due to the $N-NS$ transition which formed part of the background below T_{N-I} . The dotted curve in Fig. 3 represents the sum of the heat capacity associated with the $N-I$ transition and the background obtained in this manner. It should be noted that the first term still has a divergence at the $N-NS$ transition arising from the correction to the scaling term. However, due to a relatively small value of D , this divergence becomes noticeable only very close to T_{N-NS} . Points in close proximity to T_{N-NS} were discarded to obtain the dotted line in Fig. 3. A tangent drawn at the low end of the dotted curve and shown by a dashed line serves as the background for the $N-I$ transition below T_{N-I} . A straight (dashed) line was drawn through the data several kelvins above the $N-I$ transition to estimate the background above T_{N-I} . The two backgrounds, above and below T_{N-I} , did not match at the transition. A step change at T_{N-I} was assumed. The heat capacity in the proximity of the $N-I$ transition, within ± 1 K for 43.6 wt. %, is shown in Fig. 9(a). The

same procedure was followed for the other concentrations.

A significant pretransitional increase in C_p is evident on both sides of the $N-I$ transition. The straight top results due to $N-I$ coexistence. Sharp drops on both sides of the peak, approximated by straight lines, mark the beginning and the end of the coexistence. The shaded area under the curve and between the straight vertical lines represents the latent heat of transition ΔH . The area under the C_p curve but outside the coexistence region is the integral of the pretransitional heat capacity $\delta H = \int C_p dT$. The values of ΔH calculated for all mixtures are listed in Table II.

An unacceptable feature encountered in the above method is that it gave a lower background below the $N-I$ transition than the background above it, in apparent contradiction to the mean-field models [18] of the $N-I$ transition. Evidently, this is due to the difficulty in determining the background in the presence of the $N-NS$ transition. A *second method*, based on accepted procedures [19] of determining the background under similar circumstances, was adopted. In this case, the first term of Eq. (1) with values of parameters from the fit to the $N-NS$ transition was subtracted from the entire data. A tangent to the data well below T_{N-I} served as the background. This background was higher than the background above T_{N-I} as expected for mean-field behavior. The data and the background for the 43.6 wt. % sample are shown in

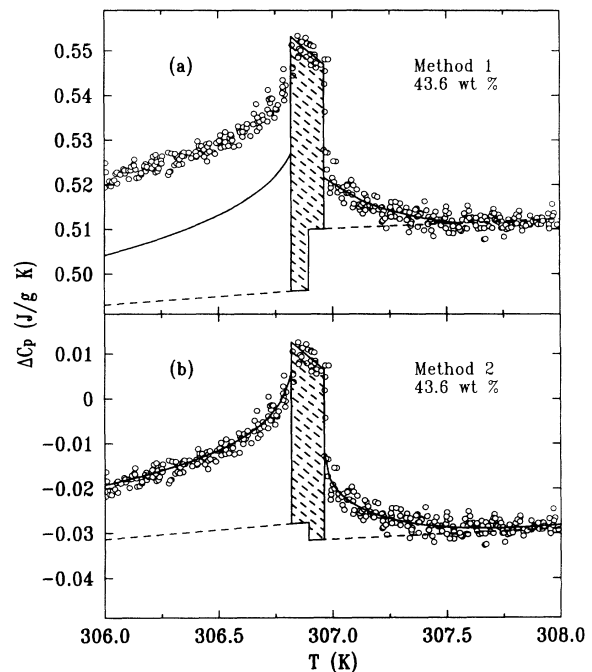


FIG. 9. ΔC_p near the $N-I$ transition of 43.6 wt. % solution shown on an expanded scale. The dashed line is the background used to calculate the transition enthalpy (total area under the solid curve) and the latent heat (shaded area) as explained in the text. The backgrounds, shown by the dashed lines, were estimated by (a) the first and (b) second method described in the text.

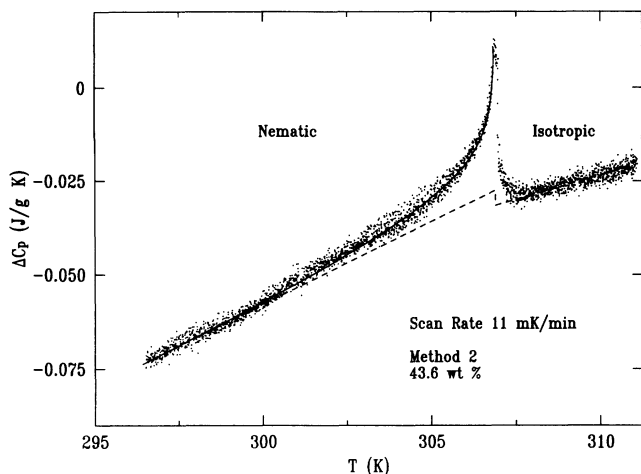


FIG. 10. Measured heat capacity, with the divergent heat capacity [first term in Eq. (1)] corresponding to the N -NS transition subtracted, as a function of temperature. The dashed lines represent the background for the N - I transition.

Fig. 9(b) over ± 1 K of T_{N-I} , and in Fig. 10 over a wide temperature range. The data and the background curves for the 48.3 and 55.3 wt. % samples, within ± 1 K of T_{N-I} , are shown in Fig. 11. Once again, the latent heat and the total transition enthalpy were calculated for all samples. The values of ΔH and δH thus obtained are also included in Table II. ΔH and the width of the coexistence region are plotted against concentration in Fig. 12. It should be pointed out that these values have a systematic deviation from, and are within 20% of, the values obtained with the first method. Although the absolute values are different depending on the method of analysis, any inferences based on the trends with concentration are, nevertheless, valid.

RESULTS AND DISCUSSION

The heat-capacity scans of CsPFO solutions in water at 39.3, 43.6, 48.3, 49.0, 50.7, 52.0, and 55.3 wt. % concentrations are shown in Figs. 3–5. Evidently, there are strong pretransitional increases in C_p at the N - I and N -

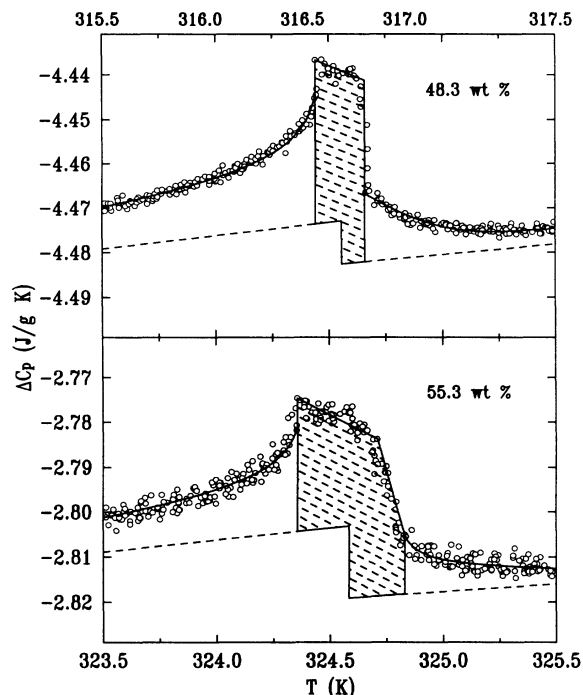


FIG. 11. ΔC_p within ± 1 K of the N - I transition of 48.3 and 55.3 wt. % samples. The dashed line is the background for calculating the transition enthalpy and the latent heat, obtained by the second method explained in the text. The horizontal scale on the top corresponds to 48.3 wt. % sample.

NS transitions. The height of the C_p peaks at the N -NS transition appear to grow with the CsPFO concentration while the height of the N - I peak remains nearly constant. These peak heights for the 43.6 wt. % solution are in excellent agreement with the results of Ref. [12] on a 41 wt. % solution. Since the background slope had to be instrumentally readjusted for each sample, its dependence on the concentration can not be inferred.

Nematic–neat-soap transition

Changes in the heat capacity below T_{N-I} are well described by Eq. (1). The ratio of heat-capacity amplitudes

TABLE II. Measured values of the latent heat (ΔH), and the nematic to isotropic transition enthalpy ($\Delta H + \delta H$) for cesium per-fluoro-octanoate plus water mixtures. Two different methods were used as discussed in the text. ΔH and ($\Delta H + \delta H$) are estimated to be accurate to $\pm 10\%$.

Conc. (wt. %)	$T_{N-I} - T_c^*$ (mK) ^a	Method 1		Method 2	
		ΔH (J/g)	ΔH (J/g)	$\Delta H + \delta H$ (J/g)	
39.3	18	5.10×10^{-3}	4.25×10^{-3}	4.85×10^{-2}	
43.6	31	6.50×10^{-3}	5.76×10^{-3}	5.74×10^{-2}	
48.3	81	9.00×10^{-3}	8.56×10^{-3}	5.04×10^{-2}	
49.0	96	9.30×10^{-3}	8.78×10^{-3}	5.57×10^{-2}	
50.7	137	1.05×10^{-2}	9.53×10^{-3}	4.90×10^{-2}	
52.0	179	1.17×10^{-2}	1.00×10^{-2}	5.36×10^{-2}	
55.3	340	1.47×10^{-2}	1.30×10^{-2}	5.09×10^{-2}	

^aObtained by linear interpolation from values in Ref. [5].

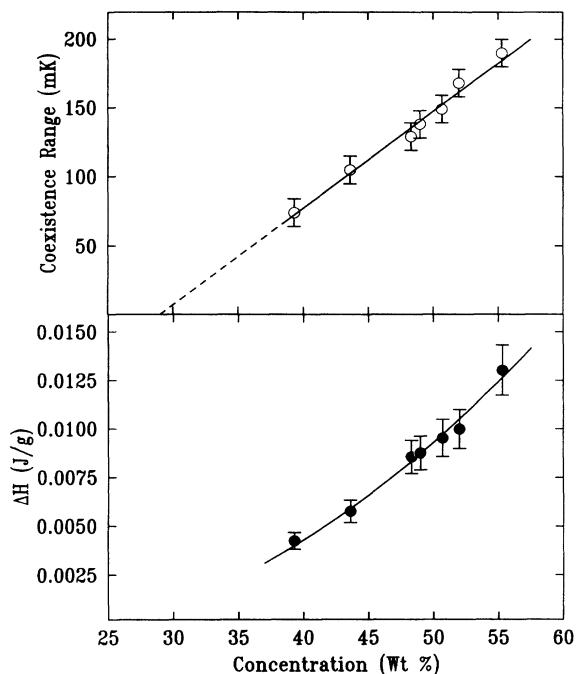


FIG. 12. Dependence of the N - I coexistence range and ΔH on the concentration of CsPFO. The solid curves are straight line (coexistence range) and quadratic fits (ΔH).

and the value of α are essentially the same as for all concentrations. There is no significant increase in the value of α at higher concentrations to suggest an approach to the predicted tricritical point. Discontinuous changes (jumps) in C_p , normally associated with the latent heat of first-order transitions, are not observed even at the highest concentration. Additionally, there is no significant narrowing of the nematic range (Fig. 1) with increasing surfactant concentration. This is invariably observed (e.g., in thermotropic materials) as a tricritical point is approached. The observed coexistence must, therefore, be attributed to other factors, such as impurities. It should be noted that the situation here is not unique. Similar impurity-induced coexistence and rounding of transitions has been observed in thermotropic materials 8OCB [13] and 4-(*n*-octyl)-4'-cyanobiphenyl (8CB) [20]. The most probable source of impurities appears to be CsPFO which, due to its own ionic nature, is likely to absorb and retain ionic impurities, in spite of best efforts to purify it. The observed increase in the coexistence range with higher surfactant concentration, and hence higher impurity content, is consistent with this conclusion. We conclude that the observed coexistence [1,10], which led to the prediction of a tricritical point, was most likely induced by impurities.

For all mixtures, the ratio of heat-capacity amplitudes (A^+/A^-) remains near unity and essentially equal to the prediction (1.005) of the 3D-XY model [21]. Although α is not exactly equal to the value (-0.007) predicted for 3D-XY-like behavior, it is quite close to it. Within experimental errors, the value of α (≤ 0.006) is consistent with the value (0.02 ± 0.17) calculated from the

correlation length exponents obtained from light scattering [2] using the hyperscaling relation. Similar results have been reported for the nematic-to-smectic- A phase transition in several thermotropic materials [26], e.g., $\bar{6}O10 + \bar{6}O8$ [22], $\bar{8}S5$ [23], T7 [23], and T8 [23], otherwise known to exhibit 3D-XY behavior.

The nematic-isotropic transition

The total enthalpy change associated with the N - I transition remains nearly constant for all mixtures while the latent heat of transition decreases as the concentration is lowered. The relative constancy of ($\Delta H + \delta H$) has a simple explanation. As the concentration is lowered, the N - I coexistence range decreases allowing measurements to be made closer to the virtual second-order transition (superheating) temperature T_c^{**} . The pretransitional fluctuations become more pronounced near this temperature and a larger δH is measured, nearly compensating for the decrease in ΔH . Consequently, the total transition enthalpy appears to be constant even though the coexistence region width and latent heat become smaller. These results suggest that a Landau point, at which the latent heat will vanish and the transition will become second order, is approached at low concentrations. The narrowing coexistence range with lower concentrations also supports this assumption. Our results are consistent with previous [5] light-scattering and magnetic-birefringence measurements. Linear extrapolation of the coexistence width vs concentration curve (Fig. 12) yields a concentration of ~ 28 wt. % for the Landau point. Unfortunately, T_{N-I} at 28 wt. % is estimated to be ~ 287 K, very near to the Krafft temperature [24] at which the solution freezes. Thus, the Landau point appears to be physically inaccessible. The latent heat of transition follows a quadratic dependence on the CsPFO concentration shown by the (solid line) fit in Fig. 12. This is very similar to the dependence observed near the N-smectic- A tricritical point [20,22] in thermotropic liquid crystals, such as 9CB+10CB and $\bar{6}O10 + \bar{6}O12$ mixtures [26].

The dependence on concentration of ΔH and of the difference [$T_{N-I} - T_c^*$] between T_{N-I} and the supercooling temperature T_c^* , taken from Ref. [5], allows us to calculate the coefficients of the Landau free-energy expansion. In the Landau-de Gennes [18] theory, the free-energy density for a uniaxial nematic can be written as

$$f = f_0 + \frac{1}{2}AS^2 - \frac{1}{3}BS^3 + \frac{1}{4}CS^4. \quad (2)$$

The scalar nematic order parameter S is defined as $\frac{1}{2}\langle(3\cos^2\theta - 1)\rangle$. Here, θ is the angle between the molecular symmetry axes (molecular long axes for thermotropic liquid crystals) and the director, and the coefficient $A = a[T - T_c^*]$, with T_c^* the virtual second-order transition temperature (or absolute stability limit of the isotropic phase). It can be easily shown [22] that the latent heat (ΔH), the discontinuity in the order parameter (ΔS_{N-I}) at T_{N-I} , and [$T_{N-I} - T_c^*$] are related to the coefficients of the Landau expansion by the following relations:

$$\Delta H = [2aB^2/9C^2]T_{N-I},$$

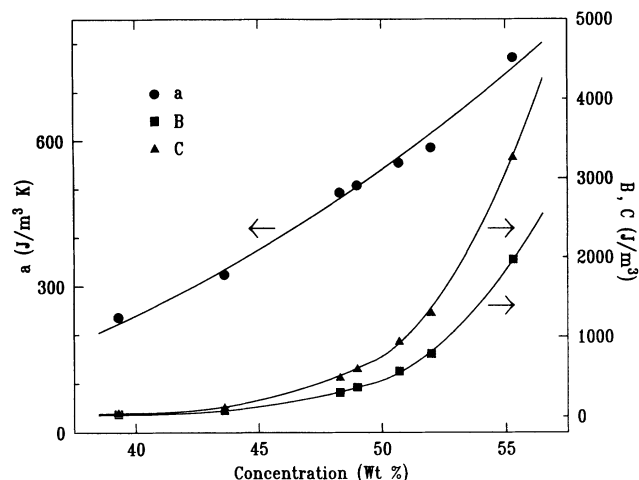


FIG. 13. Evolution of the Landau coefficients a , B , and C with CsPFO concentration. The coefficients B and C rapidly drop by two orders of magnitude and approach zero in the vicinity of the Landau point. The lines are drawn as a guide to the eye.

$$\Delta S_{N-I} = 2B/3C,$$

and

$$T_{N-I} - T_c^* = 2B^2/9aC.$$

To calculate a , B , and C , we use the values of ΔH obtained with the second method and the values of $[T_{N-I} - T_c^*]$ (also listed in Table II) calculated for these concentrations by linearly interpolating the results of a previous magnetic birefringence study [5]. The value of ΔS_{N-I} is assumed to be equal to 0.40 as predicted by Meier-Saupe [25] and found to be the approximate value for most thermotropic materials. The calculated values of the coefficients a , B , and C , are plotted in Fig. 13 as a function of concentration and given in Table III.

The coefficients of the Landau expansion decrease with concentration as the Landau point is approached. The coefficients B and C drop by two orders of magnitude while a decreases only by a factor of 3. The vanishing values of these coefficients in the neighborhood of the Landau point underscore the need to use higher-order terms [22] in Eq. (2), for a better description of this transition.

TABLE III. The Landau coefficients a , B , and C for the nematic to isotropic transition in cesium per-fluoro-octanoate plus water mixtures.

Conc. (wt. %)	a [$J/(m^3 K)$]	B (J/m^3)	C (J/m^3)
39.3	2.36×10^2	3.19×10^1	5.32×10^1
43.6	3.24×10^2	7.53×10^1	1.26×10^2
48.3	4.93×10^2	3.00×10^2	5.00×10^2
49.0	5.08×10^2	3.66×10^2	6.11×10^2
50.7	5.55×10^2	5.70×10^2	9.52×10^2
52.0	5.86×10^2	7.87×10^2	1.31×10^3
55.3	7.71×10^2	1.97×10^3	3.28×10^3

SUMMARY

We have presented a quantitative analysis of the heat capacity at the N - NS and N - I phase transitions in a lyotropic liquid crystal. By studying binary solutions of seven different concentrations, we found the behavior at the N - NS transition to be closest to a 3D- XY -like system. There was no increase in the value of α toward the tricritical value of $\frac{1}{2}$ at high concentrations. The rounding of the transition and the N - NS coexistence observed at high concentrations are attributable to impurities. The latent heat of transition and the N - I coexistence region become small in dilute solutions and, as determined by extrapolation of our results, should vanish at a Landau point at ~ 28 wt. % CsPFO concentration. It was also shown that the coefficients B and C decrease rapidly upon approach to the Landau point. We conclude that higher (than biquadratic)-order terms must be used in the Landau free-energy density expansion to adequately describe this transition.

ACKNOWLEDGMENTS

The authors wish to thank C. Garland, J. D. Litster, J. Theon, and G. Nounesis for helpful discussions. The material (CsPFO) used in this study was synthesized under Grant No. DMR-88-18561 from the National Science Foundation, and computing resources for data analysis were provided by the Ohio Supercomputer Center. This work was supported by the National Science Foundation under Grant No. DMR-88-19680.

- [1] N. Boden, P. H. Jackson, K. McMullen, and M. C. Holmes, *Chem. Phys. Lett.* **65**, 476 (1979).
- [2] B. D. Larson, Ph.D. dissertation, Massachusetts Institute of Technology, 1986; T. Haven, K. Radley, and A. Saupe, *Mol. Cryst. Liq. Cryst.* **75**, 87 (1981).
- [3] S. Kumar, L. J. Yu, and J. D. Litster, *Phys. Rev. Lett.* **50**, 1672 (1983).
- [4] S. Kumar, J. D. Litster, and C. Rosenblatt, *Phys. Rev. A* **28**, 1980 (1983).
- [5] S. Kumar, J. Brock, M. Sutton, and J. D. Litster, in *Sur-*

factants in Solution, edited by K. L. Mittal (Plenum, New York, 1989), Vol. 8, p. 35.

- [6] T. Haven, D. Armitage, and A. Saupe, *J. Chem. Phys.* **75**, 352 (1981); M. W. Wong, Ph.D. dissertation, Massachusetts Institute of Technology, 1986.
- [7] M. C. Holmes and J. Charvolin, *J. Phys. Chem.* **88**, 810 (1984); N. Boden, S. A. Corne, M. C. Holmes, P. H. Jackson, D. Parker, and K. W. Jolly, *J. Phys. (Paris)* **47**, 2135 (1986).
- [8] Y. Hendriks, J. Charvolin, M. Rawiso, L. Liebert, and M.

- C. Holmes, *J. Phys. Chem.* **87**, 3991 (1983); Y. Hendrikx, J. Charvolin, and M. Rawiso, *Phys. Rev. B* **33**, 3534 (1986).
- [9] P. J. Photinos, L. J. Yu, and A. Saupe, *Mol. Cryst. Liq. Cryst.* **67**, 277 (1981); N. Boden, D. Parker, and K. W. Jolley, *ibid.* **152**, 121 (1987).
- [10] N. Boden, K. W. Jolley, and M. H. Smith, *Liq. Cryst.* **6**, 481 (1989).
- [11] C. Chiang, C. W. Garland, S. Kumar, B. D. Larson, J. D. Litster, and C. Rosenblatt (unpublished); C. W. Garland, *Thermochim. Acta* **88**, 127 (1985).
- [12] S. Imaizumi and C. W. Garland, *J. Phys. Soc. Jpn.* **58**, 597 (1989).
- [13] D. L. Johnson, C. F. Hayes, R. J. DeHoff, and C. A. Schantz, *Phys. Rev. B* **18**, 4902 (1978); G. B. Kasting, C. W. Garland, and K. J. Kasting, *J. Phys. (Paris)* **42**, 879 (1980); J. D. Lagrange and J. M. Mochel, *Phys. Rev. Lett.* **45**, 35 (1980).
- [14] S. T. Shin and S. Kumar, *Phys. Rev. Lett.* **66**, 1062 (1991).
- [15] P. Photinos and A. Saupe, *J. Chem. Phys.* **90**, 5011 (1989).
- [16] A. Aharony and M. E. Fisher, *Phys. Rev. B* **27**, 4394 (1983); F. J. Wegner, *ibid.* **5**, 4529 (1972).
- [17] M. E. Fisher, *Phys. Rev.* **176**, 257 (1968); M. E. Fisher and P. E. Scesney, *Phys. Rev. A* **2**, 825 (1970).
- [18] P. G. deGennes, *The Physics of Liquid Crystals* (Oxford University Press, London, 1974); *Phys. Lett.* **30A**, 454 (1969); *Mol. Cryst. Liq. Cryst.* **12**, 193 (1971).
- [19] P. Das, G. Nounesis, C. W. Garland, G. Sigaud, and N. H. Tinh, *Liq. Cryst.* **7**, 883 (1990), and references therein.
- [20] G. B. Kasting, K. J. Lushington, and C. W. Garland, *Phys. Rev. B* **22**, 321 (1980); J. Theon, H. Marynissen, and W. Van Dael, *Phys. Rev. A* **26**, 2886 (1982).
- [21] J. C. Le Guillou and J. Zinn-Justin, *Phys. Rev. Lett.* **39**, 95 (1977); *Phys. Rev. B* **21**, 3976 (1980).
- [22] M. A. Anisimov, *Mol. Cryst. Liq. Cryst. A* **162**, 1 (1988), and references therein.
- [23] D. Brisbin, R. DeHoff, T. E. Lockhart, and D. L. Johnson, *Phys. Rev. Lett.* **43**, 1171 (1979), K. W. Evans-Lutterodt, J. W. Chung, B. M. Ocko, R. J. Birgeneau, C. Chiang, C. W. Garland, E. Chin, J. Goodby, and N. H. Tinh, *Phys. Rev. A* **36**, 1387 (1987).
- [24] At or below Krafft point (or temperature) micelles are insoluble; see R. C. Murray and G. S. Hartley, *Trans. Faraday Soc.* **31**, 183 (1935).
- [25] V. W. Meier and A. Saupe, *Z. Naturforsch. A* **15**, 287 (1960).
- [26] $\overline{6O8}$, $\overline{6O10}$, and $\overline{6O12}$ are 6th, 10th, and 12th members of the homologous series 4'-alkyloxy-phenyl-4-hexyloxybenzoate; $\overline{8S5}$: 4-pentylphenylthio-4'-octyloxybenzoate; 9CB and 10CB are members of the series 4'-alkyl-4-cyanobiphenyl; and T7 and T8 belong to the series 4'-(4''-alkyloxybenzyloxy)-4-cyano-stilbene.